

Article

Crystal Structure of the Substrate-Binding Domain from *Listeria monocytogenes* Bile-Resistance Determinant BilE

Stephanie J. Ruiz, Gea K. Schuurman-Wolters and Bert Poolman *

Department of Biochemistry, Groningen Biomolecular Sciences and Biotechnology Institute & Zernike Institute for Advanced Materials, University of Groningen, Nijenborgh 4, 9747 AG Groningen, The Netherlands; s.j.ruiz@rug.nl (S.J.R.); g.k.schuurman-wolters@rug.nl (G.K.S.-W.)

* Correspondence: b.poolman@rug.nl; Tel.: +31-50-363-3385; Fax: +31-50-363-4165

Academic Editors: Helmut Cölfen and Albert Guskov

Received: 28 October 2016; Accepted: 6 December 2016; Published: 9 December 2016

Abstract: BilE has been reported as a bile resistance determinant that plays an important role in colonization of the gastrointestinal tract by *Listeria monocytogenes*, the causative agent of listeriosis. The mechanism(s) by which BilE mediates bile resistance are unknown. BilE shares significant sequence similarity with ATP-binding cassette (ABC) importers that contribute to virulence and stress responses by importing quaternary ammonium compounds that act as compatible solutes. Assays using related compounds have failed to demonstrate transport mediated by BilE. The putative substrate-binding domain (SBD) of BilE was expressed in isolation and the crystal structure solved at 1.5 Å. Although the overall fold is characteristic of SBDs, the binding site varies considerably relative to the well-characterized homologs ProX from *Archaeoglobus fulgidus* and OpuBC and OpuCC from *Bacillus subtilis*. This suggests that BilE may bind an as-yet unknown ligand. Elucidation of the natural substrate of BilE could reveal a novel bile resistance mechanism.

Keywords: *Listeria monocytogenes*; ABC transporters; ABC importers; substrate-binding protein; substrate-binding domain; bile resistance; lmo1421; lmo1422

1. Introduction

Listeria monocytogenes is a Gram-positive bacterium that causes listeriosis, a potentially fatal disease which imposes a significant global burden [1]. Infection usually occurs via contaminated food, in particular ready-to-eat varieties [2,3]. The success of *Listeria monocytogenes* as a food-borne pathogen is aided by its ability to survive and grow in extreme conditions found both in food-preparation environments and in the gastrointestinal tract e.g., at low temperatures (down to -0.4 °C), at high salt concentrations (up to 10% *w/v* NaCl), or in the presence of bile [4–7]. Determining the molecular mechanisms by which *Listeria monocytogenes* survives these stresses could help to understand and control its proliferation and is thus of interest from a food safety and health perspective. It is also relevant to the rational design of probiotic bacteria [8,9].

One of the major challenges to bacterial growth and survival in the gastrointestinal tract is the presence of bile (for reviews, including mechanisms of toxicity and bacterial resistance, see References [10–13]). Bile is a digestive secretion produced by the liver and stored and concentrated in the gallbladder before being released into the lower intestine, where it aids in the emulsification and solubilization of fats. This is achieved by bile acids (also referred to as bile salts or bile alcohols, Figure S1), a class of amphipathic cholesterol-derived steroids, which are also potent antimicrobials due to their activity against biological membranes [12,14]. Several bile resistance mechanisms have been identified in *Listeria monocytogenes* and other bacteria including the expression of multidrug resistance efflux pumps and modification of bile acids via the enzyme bile salt hydrolase [6,7,15–18].

Listeria monocytogenes BilE is a putative ATP-binding cassette (ABC) transporter that promotes bile tolerance *in vitro* and colonization of the gastrointestinal tract *in vivo* [15,16,18]. However, the specific mechanism(s) by which it achieves this is unknown. There are many transporters known to mediate bacterial stress responses and virulence through the uptake of compatible solutes, low molecular weight osmolytes that can be accumulated to high concentrations without interfering with cellular processes [19]. In *Listeria monocytogenes*, the ABC transporters Gbu and OpuC, which are homologous to BilE, as well as the functionally related secondary transporter BetL, contribute to osmo-, bile- and chill-tolerance by importing glycine betaine and carnitine [16,20–22]. Although it was initially hypothesized that BilE (then called OpuD) was an additional compatible solute transporter, it has since been demonstrated that it is unable to mediate transport of glycine betaine, carnitine, or choline (a metabolic precursor of glycine betaine), and plays no role in osmo- or chill-tolerance [18]. The observation that *Listeria monocytogenes* knockout cells accumulate lower levels of the bile component chenodeoxycholic acid led to the description of BilE as a bile exclusion system [18,23]. This is at odds with the similarity of BilE to Type I ABC importers, which are structurally and evolutionarily distinct from ABC exporters [24,25].

The main aim of this study was to generate structural information on BilE in order to make improved hypotheses about the mechanism(s) by which it mediates bile resistance. The soluble C-terminal domain of BilEB was crystallized and confirmed to have a substrate-binding protein fold belonging to structural subcluster F-III [26,27]. The characterized members of this group are all associated with ABC importers and bind compatible solutes. Although amino acid residues interacting directly with the substrate are largely conserved with characterized homologs, differences in surrounding residues mean that the overall architecture of the binding site varies significantly.

2. Results and Discussion

2.1. Sequence Analysis

BilE is encoded by the genes *lmo1421* and *lmo1422* in a genetic arrangement similar to the OpuA (BusA) system from *Lactococcus lactis* [28,29] (Figure 1A,C). The first gene in the operon encodes BilEA, the nucleotide-binding domain (NBD). The second gene encodes BilEB, a fusion protein containing both a transmembrane (TMD) domain and a substrate-binding domain (SBD). The predicted functional transporter is a homodimer (Figure 1B). Although the architecture of BilE is similar to *Lactococcus lactis* OpuA, the individual domains share more sequence similarity with the equivalent subunits from *Listeria monocytogenes* OpuC [30], *Bacillus subtilis* OpuB and OpuC [31], and *Archaeoglobus fulgidus* ProX [32,33] (Figure 1C). These are all Type I ABC importers that contribute to osmo- or thermotolerance through the import of quaternary ammonium compounds (QACs) which act as compatible solutes either directly (e.g., glycine betaine), or as metabolic precursors (e.g., choline).

Part of the justification for reclassifying BilE as a bile exporter was the identification of “bile acid permease signature sequences” conserved between BilEA and the NBDs of bile salt exporters *Saccharomyces cerevisiae* Ybt1 and mammalian ABCB11 [18]. We constructed an expanded sequence alignment, which includes the NBDs OpuCA and GbuA from *Listeria monocytogenes*, and see no evidence that BilEA shares unique sequence characteristics with the eukaryotic proteins (Figure 1D and Figure S2).

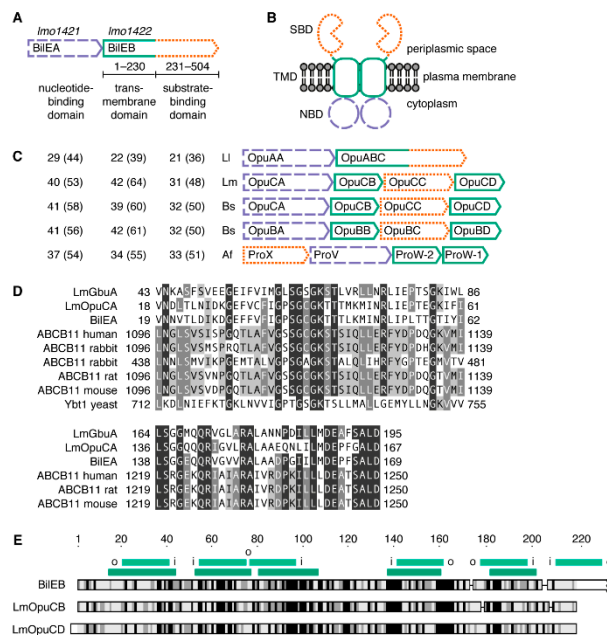


Figure 1. (A) The genetic arrangement of Bile; (B) a schematic of the predicted functional transporter; and (C) comparison to characterized homologs. Strain details and protein accession numbers are listed in Table A1. Genes and proteins are color-coded based on the predicted function: nucleotide-binding domains (NBDs), purple long dashes; transmembrane domains (TMDs), solid green; substrate-binding domains (SBDs), orange short dashes. When two TMDs are present, values from the closest match are reported. Numbers indicate the percentage sequence identity (similarity) between equivalent domains based on pairwise alignments made with the program needle from EMBOSS (the European Molecular Biology Open Software Suite) [34]. (D) An extract from a multiple sequence alignment of selected NBDs. The region shown is the same as in Sleator et al. [18], but the alignment has been expanded to include proteins from the *Listeria monocytogenes* Gbu and OpuC systems. Residues are shaded according to percentage sequence identity. (E) Multiple sequence alignment of BileB and the TMDs from *Listeria monocytogenes* OpuC. Numbering is according to BileB. Sequences are shaded according to percentage sequence similarity. Bars above the alignment indicate transmembrane segments (TMSs) predicted by TOPCONS [35] (light green) or by comparison to crystal structures of homologous ABC importers (dark green). Lettering indicates the orientation of predicted TMSs relative to the cytoplasm (out-to-in or in-to-out), which is in agreement between the two methods.

In the ABC transporters that have been crystallized, the fold of the TMD varies significantly between importers and exporters [24]. The HHPred server [36], which is designed for remote protein homology detection and structure prediction, was used to search the Protein Data Bank (PDB) with residues 1–231 of BileB as the query sequence. The top matches were to the permease subunits of six different Type I ABC importers from bacteria and archaea (Table A2). The sequence alignment produced by HHPred covers the five transmembrane segments (TMSs) that are conserved between all of these structures and which, after dimerization, make up the core of the transporter. The predicted positions of these TMSs in BileB closely match topology predictions made using the TOPCONS server [35] (Figure 1E). The additional sixth TMS, predicted by TOPCONS, would position the predicted C-terminal SBD at the outer surface of the membrane where it could serve as receptor and bind ligands for subsequent transport. A comparison of BileB with OpuCB and OpuCD from *Listeria monocytogenes* shows that the TMDs are similar in size, and that there is sequence similarity along the entire domain (Figure 1E).

Based on sequence homology, the C-terminus of BileB contains a substrate-binding domain (SBD) belonging to substrate-binding protein (SBP) subcluster F-III [26,27]. All characterized members of this cluster are part of an ABC transporter and bind QACs via cation– π interactions. They can be further

divided into two groups based on whether the quaternary ammonium of the substrate is coordinated via three tryptophan residues (e.g., OpuAC from *L. lactis* [37] and ProX from *Escherichia coli* [38]) or four tyrosines (e.g., ProX from *Archaeoglobus fulgidus* [33]). Interestingly, a sub-group also exists which share their tertiary structure with the *Lactococcus lactis* OpuAC group (including tryptophan residues of the binding site) but in whose primary sequence the N- and C-terminal halves are swapped (e.g., OpuAC from *Bacillus subtilis* [39,40]). The sequence of BilEB is most similar to AfProX (33% identity, 51% similarity), although one binding site tyrosine is substituted for a phenylalanine. Figure 2 shows a multiple sequence alignment of BilEB, AfProX, and other selected homologs in which these four tyrosine residues are conserved: OpuBC and OpuCC from *Bacillus subtilis* [31]; OpuCC from *Listeria monocytogenes* [30], *Staphylococcus aureus* [41], *Pseudomonas aeruginosa* and *Pseudomonas syringae* [42]; OsmX (OpuCC) from *Salmonella typhimurium* [43,44]; and YehZ from *Escherichia coli* [45]. The known ligands of these proteins include glycine betaine, proline betaine, choline, acetylcholine, choline-*O*-sulfate, carnitine, and ectoine (Figure S3). Several other studied homologs were excluded from this analysis: OpuCC from *Pseudomonas syringae* pv. *syringae* B728a [42], because it is 97% identical to the included OpuCC from *Pseudomonas syringae* pv. *syringae* DC3000; YehZ from *Salmonella typhimurium* [46], because it is 88% identical to EcYehZ and its substrate is unknown; and ProX from *Agrobacterium tumefaciens*, because no data apart from crystal structures (PDB ID 4NE4 and 4ND9) are available.

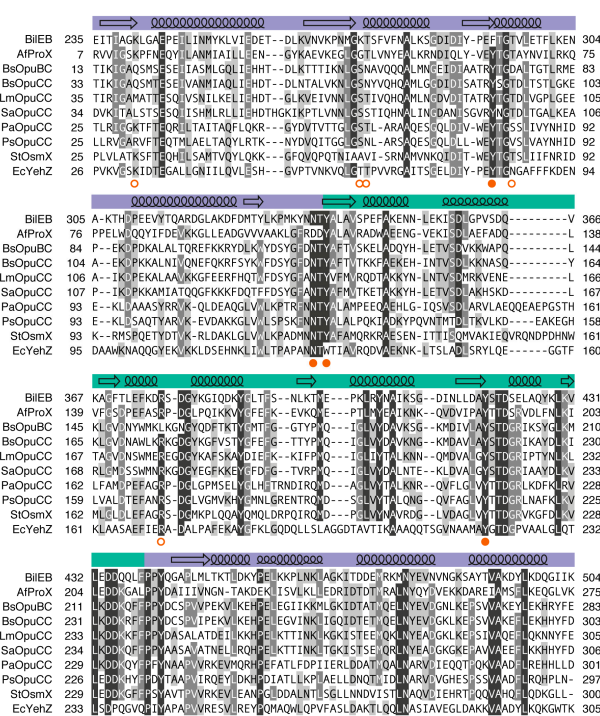


Figure 2. Multiple sequence alignment of BilEB and selected substrate-binding protein homologs. For a full list of organism names and protein accession numbers, see Table A1. The alignment has been truncated at the N-terminus to exclude signal sequences and residues not visible in the crystallographic structures. Sequences are numbered according to the unprocessed form of the protein, unless this varies from numbering used in published studies in which case the numbering is consistent with the literature. Residues are shaded according to percentage sequence identity. The secondary structure of BilEB_{SD} is indicated above the alignment. Domain A is indicated in purple, domain B in green. Arrows indicate β -sheets; large loops indicate α -helices, small loops indicate 3_{10} -helices (secondary structure assigned by DSSP [47]). Orange symbols below the alignment indicate amino acid residues involved in substrate binding either through caging the quaternary ammonium (closed circles) or forming salt bridges or hydrogen bonds (open circles).

2.2. Structure of the Putative Substrate-Binding Domain from BilEB

We were unable to measure any glycine betaine transport or osmoprotective activity when BilE was expressed in *Lactococcus lactis* (data not shown). We decided to focus on the putative substrate-binding domain (residues 231–504 of BilEB, hereafter referred to as BilEB_{SBD}). BilEB_{SBD} was successfully expressed in *Escherichia coli* with a His-tag and purified from the soluble fraction via affinity chromatography. The purified protein was analyzed by SEC-MALLS (size-exclusion chromatography coupled to static light-scattering, differential refractive index, and UV absorbance measurements) in order to determine its oligomeric state [48]. A single elution peak was observed with an estimated molecular mass of 32.4 kDa (Figure S4). This is in good agreement with the molecular mass of 33.4 kDa calculated using the ProtParam tool [49] and indicates that the isolated BilEB_{SBD} is monomeric in solution. Differential scanning calorimetry was used to screen for substrate binding, but no significant changes in melting temperature were observed in the presence of glycine betaine, carnitine, choline, proline, or cholate (5 μ M of protein and up to 5 mM of ligand at pH 7.5; data not shown).

The X-ray structure of BilEB_{SBD} was determined at a resolution of 1.5 Å and deposited in the PDB under accession number 4Z7E (Table 1). Two protein molecules are present in the asymmetric unit but they differ only slightly, with a root-mean-square deviation of atomic positions (RMSD) of 0.33 Å over all atoms. Several areas of density were assigned to polyethylene glycol and propanoic acid from the crystallization solution, but for the most part these are external to the protein and are not biologically relevant. The exception is a molecule of propanoic acid in the putative binding site of BilEB_{SBD}, which will be discussed in the following section.

Table 1. Data collection, phasing and refinement statistics ¹.

Data Collection	
Space group	P21
Cell dimensions	
<i>a</i> , <i>b</i> , <i>c</i> (Å)	45.96, 62.87, 97.02
α , β , γ (°)	90, 91.71, 90
Resolution range (Å)	48.5–1.50 (1.54–1.50)
Unique reflections	166,913
<i>R</i> _{merge}	0.025 (0.80)
$\langle I/\sigma(I) \rangle$	13.1 (1.04)
CC _{1/2}	99.9 (47.6)
Completeness (%)	96.0 (97.0)
Redundancy	1.9 (2.0)
Refinement	
Resolution range (Å)	48.49–1.50 (1.52–1.50)
No. of reflections, working set	166,898 (5303)
No. of reflections, test set	8333 (280)
<i>R</i> _{work} / <i>R</i> _{free}	0.153/0.198
No. of non-H atoms	
Protein	4298
Ligand	66
Water	470
Total	4834
Average <i>B</i> factors (Å ²)	
Protein	39.5
Ligand	65.1
Water	44.9
R.M.S. deviations	
Bonds (Å)	0.010
Angles (°)	1.242
Ramachandran statistics (%)	
Favored	98.9
Allowed	0.7
Outliers	0.4

¹ Values in parentheses are for the highest-resolution shell.

The overall fold of BilEB_{SBD} consists of two globular α/β domains joined by a hinge formed from two long flexible strands (Figure 3A). Each domain is comprised of a five-stranded β -sheet surrounded by α -helices. This fold is characteristic of SBPs of subcluster F-III [26,27]. As expected based on sequence similarity, a search for structural homologs in the PDB using the Dali server [50] gave the best match as the open, unliganded structure of AfProX (PDB ID 1SW5, Table A3). The RMSD is 1.7 Å over 267 aligned residues (out of a total of 270). Matches with Z-scores greater than 25 were also returned for the structures of SaOpuCC, AtProX, BsOpuBC, BsOpuCC, and EcYehZ (Table A3). Based on comparisons with AfProX and in keeping with the literature we have defined domain A as containing the N- and C-terminus (residues 235–338 and residues 440–504) and domain B as containing the central region of the protein (residues 339–439). The binding site of SBPs contains residues from both domains, which trap the ligand by moving towards each other in what is often described as a “Venus’s-flytrap” mechanism [51] (Figure 3B). A comparison of the BilEB_{SBD} structure with structural homologs shows that it was crystallized in the open conformation.

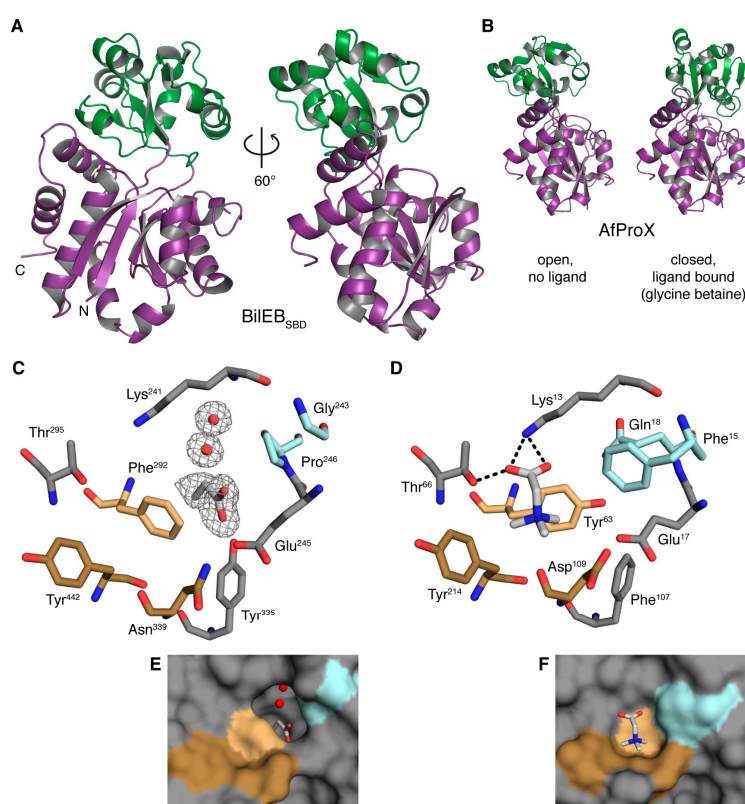


Figure 3. Comparison of the crystal structures of BilEB_{SBD} and *A. fulgidus* ProX: (A,B) BilEB_{SBD} and AfProX in cartoon representation with domain A of each protein in purple and domain B in green. Both the open and closed conformations of ProX are shown (PDB ID 1SW5 and 1SW2, respectively) in order to demonstrate the movement of domains during substrate binding. (C,D) Binding site residues from domain A of (C) BilEB_{SBD} and (D) AfProX (PDB ID 1SW5). Amino acid residues and ligands are shown in stick representation with oxygens colored red and nitrogens colored blue. Propanoic acid and glycine betaine are colored white. Bound water molecules are shown as red spheres. Residues forming a cage around the quaternary ammonium are dark gold except for the position corresponding to Phe²⁹² in BilEB_{SBD}, which is pale gold. Residues corresponding to Gly²⁴³ and Pro²⁴⁶ in BilEB_{SBD} are colored pale blue. The grey mesh in (C) is an omit Fo-Fc electron density map contoured at 2.0 σ . Dashed lines indicate hydrogen bonds or salt bridges. (E,F) The same view as (C,D), respectively, with the proteins shown in surface representation and domain B omitted for clarity. Images were prepared in PyMOL [52].

2.3. Binding Site Comparisons

AfProX, BsOpuBC and BsOpuCC have all been crystallized in complex with their natural substrates [33,53,54]. In each case the quaternary ammonium group sits in a cage whose sides are formed by four Tyr residues and whose base is the main chain of either an Asp or Asn. The other part of the substrate is coordinated by interactions with specific side-chains. In the case of AfProX, the cage is formed by Tyr⁶³, Tyr¹¹¹, Tyr¹⁹⁰, Tyr²¹⁴, and Asp¹⁰⁹, while the carboxylic tail of GB or PB forms salt bridges with Lys¹³ and Arg¹⁴⁹ (domain A and B, respectively) and a hydrogen bond with Thr⁶⁶ (domain A). These residues are conserved in BileB_{SBD} in both the primary sequence and the crystallographic model (Figures 2 and 3C), except for the substitution of Phe²⁹² for Tyr⁶³.

Studies of AfProX suggest that residues of the substrate-binding site from domain A undergo minimal conformational change between the open and closed forms of the protein [32,33]. Despite the fact that BileB_{SBD} has only been crystallized in the open, unliganded conformation, we can still make some comments about the putative binding site. A comparison of domain A from BileB_{SBD} and AfProX show that the position of the binding site residues is largely conserved (Figure 3C,D). The Phe²⁹² side chain of BileB_{SBD}, however, is tilted into the putative binding site. The corresponding residue in AfProX, Tyr⁶³, forms hydrogen bonds with Glu¹⁷ and Gln¹⁸ [33] (Figure 3D). This Glu residue is strictly conserved in characterized homologs (Figure 2) and appears to hydrogen bond with the equivalent Tyr in all the available crystal structures. Phe²⁹² is unable to form these interactions.

The positioning of Phe²⁹², as well as the substitution of Phe¹⁵ and Gln¹⁸ from AfProX with the less bulky Gly²⁴³ and Pro²⁴⁶ in BileB_{SBD}, results in a cavity on the face of domain A adjacent to the putative binding site (Figure 3E). Within this cavity is a molecule of propanoic acid bound by stacking interactions with Phe²⁹² and hydrogen bonding with Tyr³³⁵. In chain B of the model, which contains the best density for the propanoic acid, two water molecules can also be clearly seen within this cavity. These are coordinated by hydrogen bonds with the propanoic acid, the main chain carboxyl of Pro²⁹⁰, and the main chain amide of Lys²⁴¹. No such cavity is seen on the domain A face of AfProX, BsOpuBC or SaOpuCC (Figure 3F and Figure S5). BsOpuCC does have a larger binding site, but the extra space is in a different position and is required in order to accommodate the larger substrate carnitine. The structures of open, unliganded EcYehZ and AtProX, which both have an Asp and Gly at the positions equivalent to Gly²⁴³ and Pro²⁴⁶, do show a cavity in the same position as BileB_{SBD}. Although it is smaller, it is open to the bulk solvent and contains two water molecules.

The presence of Gly²⁴³ also has implications for stabilization of the closed state. In AfProX, the position of the Tyr¹⁹⁰ phenyl ring from domain B is stabilized by C–H . . . π interactions with Phe¹⁵. The structures of BsOpuBC and BsOpuCC suggest that similar interactions occur between Tyr¹⁹⁷/Tyr²¹⁷ and Met²¹/Tyr⁴¹. The mutation of Met²¹ to Ala in OpuBC results in a three-fold increase in the K_d for choline from 30 μ M to 97 μ M [53]. In the structure of BileB_{SBD} there are no nearby residues that would be able to fulfill this role.

These differences in the structure of BileB_{SBD} suggest that its natural ligand could vary significantly from those predicted based on sequence analysis. Unfortunately, the crystal structure does not lead directly to possible alternatives. Bile acids, besides being even larger than the extra space made available by the binding site cavity, do not make sense as an import substrate for a bile resistance protein; for bile acid tolerance the molecules would have to be exported rather than imported.

2.4. Conservation of BileB

In order to determine if the structural features described here are unique to BileB, we used the UniRef50 database [55] to generate a list of sequences with significant similarity to BileB_{SBD} [E-value of less than 0.0001 in a Basic Local Alignment Search Tool (BLAST) search] and less than 50% pairwise sequence identity. Each sequence in the list thus represents a cluster of one or more original sequences. Using AfProX as the query sequence resulted in a very similar list. We then excluded sequences that did not contain either a Tyr, Phe or Trp residue at the four positions corresponding to the binding site tyrosines of AfProX. Our final list of 198 sequences contains proteins with various

domain organizations including isolated SBPs as well as TMD-SBD, SBD-TMD and even SBD-SBD fusions (Figure 4A, Supplementary File S1). Analysis with HHpred [36] suggests that these additional C-terminal SBDs belong to structural subclusters F-IV or E-II, both of which contain SBPs that bind amino acids and are associated with importers, channels or receptors [26,27]. We also identified three SBPs and four TMD-SBD fusions which contain a sequence swap similar to OpuAC from *Bacillus subtilis* [39,40] (Figure 4A).

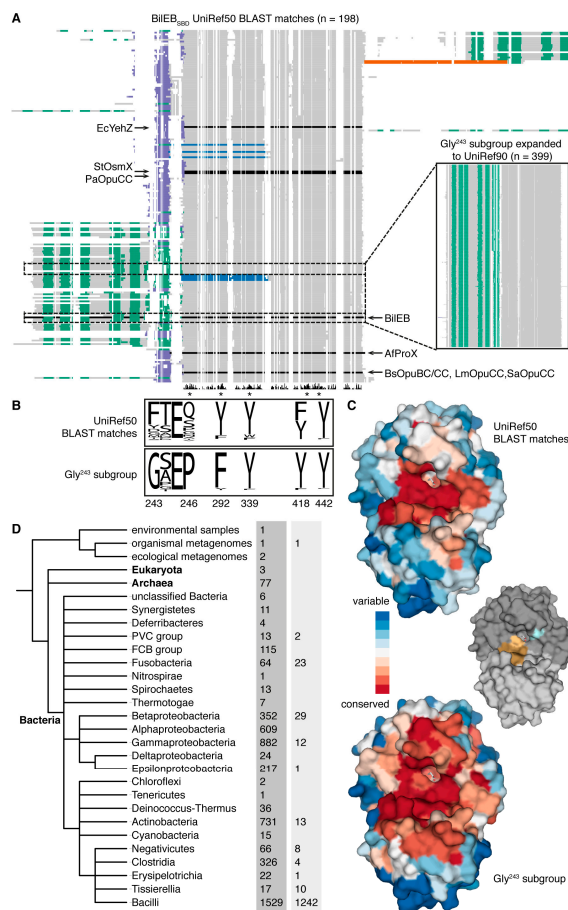


Figure 4. Conservation of BilEB: (A) Multiple sequence alignments of UniRef50 (main) and UniRef90 (inset) reference sequences. Reference sequences for clusters containing SBPs discussed in this paper are shown in black. The reference sequence for the cluster containing PsOpuCC was removed during an automated trimming step. Topology predictions made by TOPCONS [35] are shown in green (TMSs) and purple (signal sequences). Orange indicates an additional SBP fold as predicted by HHpred [36]. Where sequences were manually altered to reflect a change in the primary sequence compared to the predicted tertiary structure (as described for *Bacillus subtilis* OpuAC), the shifted C-terminal portion is shown in blue. Dashed outlines indicate sequences containing a Gly residue at the position corresponding to Gly²⁴³ of BilEB. The histogram below the main alignment shows sequence conservation. (B) Frequency plots showing the distribution of amino acids at corresponding positions of each alignment. Numbering shown is according to BilEB. (C) The ConSurf server [56] was used to map the conservation of each alignment onto the BilEB_{SBD} structure. A molecule with the same color scheme as Figure 3 is included for clarity. Domains A and B are shown in dark grey and light grey, respectively. Residues predicted to form a cage around the quaternary ammonium are dark gold except for Phe²⁹², which is pale gold. Gly²⁴³ and Pro²⁴⁶ are colored pale blue. (D) Phylogenetic distribution of the sequences represented in each alignment. Values shown are the number of unique organisms in each taxa which have sequences in the UniRef50 (left column) or UniRef90 (right column) clusters. Images were prepared using Jalview [57], PyMOL [52], and iTOL [58].

The most common residues at the position corresponding to Gly²⁴³ of BilEB are Phe (61.3%), Tyr (9.4%), Asp (7.3%), Gly (6.8%), Met (4.7%), Thr (3.1%), and Ser (2.1%) (Figure 4B). Each of these alternatives, except for Tyr, is represented in the characterized QAC-binding homologs (Figure 2). Expanding the 13 reference sequences containing a Gly at this position to the UniRef90 database (a maximum of 90% pairwise sequence identity) returned 399 sequences, all of which are TMD-SBD fusions (Figure 4A, inset, and Supplementary File S2). Gly²⁴³ (98.8%), Pro²⁴⁶ (99.0%) and Phe²⁹² (94.5%) are all highly conserved (Figure 4B). Mapping the conservation from each multiple sequence alignment onto the BilEB_{SBD} crystallographic model shows that conserved residues are clustered around the putative binding site (Figure 4C). Within the Gly²⁴³ subgroup the residues lining the cavity on the face of domain A are also conserved. This suggests that BilE is a member of a conserved subgroup with unknown transport specificity.

The initial list of UniRef50 reference sequences represents genes from a wide range of taxa, including eukaryotes, archaea and bacteria (Figure 4D). The highest number of sequences is found within the class Bacilli. The UniRef90 Gly²⁴³ subgroup shows a similar phylogenetic distribution, although it is even more heavily biased towards the Bacilli. A closer look suggests that BilE homologs are widespread within genera known to contribute to the human microbiome including *Bacillus*, *Enterococcus*, *Lactobacillus*, *Neisseria*, *Staphylococcus*, and *Streptococcus*, as well as in the genus *Lactococcus*.

3. Materials and Methods

3.1. Cloning, Expression and Purification

The isolated substrate-binding domain of BilE was expressed in *Escherichia coli* MC1061 with an N-terminal tag consisting of 10 histidine residues and a tobacco etch virus (TEV) protease cleavage site (for the full amino acid sequence see Appendix B). To construct the expression plasmid, amino acid residues 231–504 of BilEB were amplified by polymerase chain reaction using the oligonucleotides 5'-ATGGTGAGAA TTTATATTTT CAAGGTTCCG ATAAAAGGA AATTACAATT GCTGGTAAAT TAG-3' and 5'-TGGGAGGGTG GGATTTTCAT TATTTAATAA TACCTTGATC TTTCAAATAG TCTTTGGCAA CTG-3' and cloned into pBADnLIC as described by Geertsma and Poolman [59]. The resulting plasmid, pBAD-lmo1422SBDnLIC, was confirmed by sequencing the entire open reading frame.

For expression, *Escherichia coli* containing pBAD-lmo1422SBDnLIC were inoculated into LB media containing 100 µg/mL ampicillin and grown at 37 °C with shaking to an OD₆₆₀ of 0.7. L-Arabinose was added to induce expression (final concentration 5 × 10⁻³% w/v) and the cultures incubated for 2 h at 25 °C with shaking. Cells were harvested by centrifugation and resuspended in Buffer A (50 mM potassium phosphate pH 7.5, 200 mM NaCl) with 5 mM MgSO₄ and 100 µg/mL DNase. Cells were disrupted by a single pass through a cell disruptor (Constant Systems Ltd, Daventry, UK) at 25,000 psi and stored at −80 °C before purification.

BilEB_{SBD} was purified by Ni²⁺-affinity and size-exclusion chromatography using ÄKTA systems (GE Healthcare Life Sciences, Eindhoven, The Netherlands). Disrupted cells were thawed on ice and the insoluble fraction removed by ultracentrifugation (80,000 rpm, 4 °C, 20 min). The lysate was diluted 3-fold in Buffer A, and imidazole added to a final concentration of 10 mM. The solution was passed over a Ni²⁺-sepharose column (approximately 1 mL bed volume per mg wet weight cells) which had been pre-equilibrated in Buffer B (20 mM Hepes pH 7.5, 200 mM NaCl) with 10 mM imidazole. The column was washed with three volumes of Buffer B with 75 mM imidazole, and eluted with Buffer C (20 mM Hepes pH 7.5, 150 mM NaCl) with 500 mM imidazole. Elution fractions were collected directly into tubes containing 1/100 volumes of 0.5 M Na-EDTA (to give a final concentration of 5 mM) before being pooled, diluted 2.5-fold in Buffer C, and concentrated using a Vivaspin column (GE Healthcare Life Sciences, Eindhoven, The Netherlands) with a molecular weight cut-off of 10 kDa. The concentrated sample was then passed over a Superdex 200 10/300 GL column (GE Healthcare Life

Sciences, Eindhoven, The Netherlands) in Buffer C. Eluted fractions were again concentrated using a Vivaspin column.

Determination of the molecular weight of purified BilEB_{SBD} by SEC-MALLS was performed as described previously [48], using a Superdex 200 10/300 GL column pre-equilibrated in Buffer C.

3.2. Crystallization

All crystallization experiments were performed at 4 °C. Initial crystallization trials were carried out using a high-throughput crystallization robot (Mosquito, TTP Labtech, Melbourn, UK), commercially available kits from Molecular Dimensions, and the sitting-drop vapor-diffusion technique. BilEB_{SBD} was found to crystallize in condition 25 from PACT *premier* (0.1 M PCTP (sodium propionate, sodium cacodylate trihydrate, Bis-Tris propane) pH 4.0, 25% (*w/v*) PEG-1500). Further crystallization trials were carried out using the hanging-drop vapor-diffusion method. The crystal used to solve the structure was obtained by mixing equal volumes of BilEB_{SBD} (20 mg/mL in Buffer C) with the reservoir solution (0.1 M PCTP pH 4.25, 25% *w/v* PEG-1500). Cryo-buffer consisted of PACT *premier* 25 with an additional 15% (*w/v*) PEG-1500.

3.3. Structure Determination and Refinement

X-ray diffraction data were collected at the X06SA (PXI) beamline at the SLS (Paul Scherrer Institut, Villigen, Switzerland) and processed with the XDS package [60]. The structure was solved by molecular replacement with the program Phaser [61] using the structure of open, unliganded *Archaeoglobus fulgidus* ProX (PDB code 1SW5) as the search model. Refinement was performed with REFMAC5 [62] and PHENIX [63], with additional manual adjustments made in Coot [64]. The data and refinement statistics are listed in Table 1.

3.4. Sequence and Structure Analysis

Percent sequence identity values are from pairwise sequence alignments generated by the EMBOSS needle program [34]. All multiple sequence alignments were made using Clustal Omega [65] at the EMBL-EBI server [66]. Topology predictions were made using the TOPCONS server [35].

To generate a list of BilEB_{SBD} homologs with lowered redundancy, a BLAST search was conducted against the UniRef50 database (accessed 9 September 2016) [55] using residues 231–504 of BilEB as the query sequence. Sequences less than 250 or more than 650 amino acids in length were discarded. The resulting list was trimmed using MaxAlign [67], which removes sequences creating significant gaps in a multiple sequence alignment. This is designed to remove truncated or incorrectly annotated sequences, but in this case also removed several proteins that appear to have a sequence swap similar to OpuAC of *Bacillus subtilis* [39,40]. These sequences were manually altered by removing the C-terminal portion and inserting it immediately following the predicted signal sequence or final TMS, and they were then added back to the list. Finally, any sequences that did not contain a Tyr, Phe, or Trp at the four positions corresponding to the binding site Tyr residues of AfProX were discarded. The final alignment contains 198 sequences of 267 to 650 amino acids in length. The members of each UniRef50 cluster whose representative sequence has a Gly at the position equivalent to Gly²⁴³ of BilEB ($n = 13$) were gathered and reduced to 90% identity by mapping to the UniRef90 database. The same alignment and trimming procedures were applied, yielding a multiple sequence alignment with 399 sequences of 500 to 597 amino acids in length.

4. Conclusions

The C-terminus of BilE has a distinctive SBP fold, which supports the classification of BilE as a Type I ABC importer. Differences in the architecture of the binding site compared to characterized homologs indicate that the transport substrate(s) of BilE may vary significantly from those previously predicted (glycine betaine and other quaternary ammonium compounds which act as compatible solutes). This would explain why no transport activity has been observed, and opens up the possible

discovery of a novel mechanism of bile resistance. The crystal structure of BilEB_{SBD} determined in this study allows for the identification of possible candidate substrates via *in silico* methods such as ligand docking.

Supplementary Materials: The following are available online at www.mdpi.com/2073-4352/6/12/162/s1: Figure S1: Chemical structures of the most abundant bile acids in humans; Figure S2: Multiple sequence alignment of selected NBDs; Figure S3: Ligands of substrate-binding proteins homologous to BilEB_{SBD}; Figure S4: Determination of the oligomeric state of BilEB_{SBD}; Figure S5: The binding site on the face of domain A; File S1: Multiple sequence alignment of UniRef50 reference sequences; File S2: Multiple sequence alignment of UniRef90 reference sequences.

Acknowledgments: We thank Albert Guskov for assistance in the final stages of refinement and submission to the PDB. We also thank Faizah Fulyani and Andreja Vujičić Žagar for their earlier work on BilE, and Stephan Rempel and Tjeerd Pols for their help with SEC-MALLS. This work was carried out within the BE-Basic R&D Program, which was granted a FES subsidy from the Dutch Ministry of Economic Affairs, Agriculture and Innovation (EL&I). The research was also funded by NWO TOP-GO program (project number 700.10.53), NWO TOP-PUNT (project number 13.006) grants and ERC Advanced grant (ABCVolume 670578).

Author Contributions: Stephanie J. Ruiz and Bert Poolman conceived and designed the experiments; Stephanie J. Ruiz and Gea K. Schuurman-Wolters performed the experiments; Stephanie J. Ruiz analyzed the data; Bert Poolman contributed reagents/materials/analysis tools; and Stephanie J. Ruiz and Bert Poolman wrote the paper.

Conflicts of Interest: Albert Guskov, Editor of this Special Issue, lent technical assistance as outlined in the Acknowledgements. He had no role in the design of the study; in the collection, analyses, or interpretation of data; in the writing of the manuscript, or in the decision to publish the results.

Appendix A.

Table A1. Proteins used in this study for sequence- and structure-based analyses.

Organism ¹ and Transporter	Protein Subunits ^{2,3} and UniProtKB Accession Numbers			
<i>Archaeoglobus fulgidus</i> VC16 (Af)				
ProU [32,33]	ProX (SBD) O29280	ProV (NBD) O29281	ProW-2 (TMD) O29282	ProW-1 (TMD) O29283
<i>Bacillus subtilis</i> 168 (Bs)				
OpuB [31,53]	OpuBA (NBD) Q45460	OpuBB (TMD) Q45461	OpuBC (SBD) Q45462	OpuBD (TMD) P39775
OpuC [31,54]	OpuCA (NBD) O34992	OpuCB (TMD) O34878	OpuCC (SBD) O32243	OpuCD (TMD) O34742
<i>Escherichia coli</i> K-12 (Ec)				
YehZYXW [45]	YehZ (SBD) P33362	YehY (TMD) P33361	YehX (NBD) P33360	YehW (TMD) P33359
<i>Lactococcus lactis</i> subsp. <i>lactis</i> IL1403 (Ll)				
OpuA [28,29,37]	OpuAA (NBD) Q9KIF7	OpuABC (TMD-SBD) Q7DAU8		
<i>Listeria monocytogenes</i> EGD-e (Lm)				
BilE [18]	BilEA (NBD) Q7AP69	BilEB (TMD-SBD) Q8Y775		
Gbu [68]	GbuA (NBD) Q7AP76	GbuB (TMD) Q7AP75	GbuC (SBD) Q8Y898	
OpuC [30]	OpuCA (NBD) Q7AP65	OpuCB (TMD) Q7AP66	OpuCC (SBD) Q7AP67	OpuCD (TMD) Q7AP68
<i>Pseudomonas aeruginosa</i> PAO1 (Pa)				
OpuC [42]	OpuCD (TMD) Q9HXC5	OpuCC (SBD) Q9HXC4	OpuCB (TMD) Q9HXC3	OpuCA (NBD) Q9HXC2

Table A1. Cont.

Organism ¹ and Transporter	Protein Subunits ^{2,3} and UniProtKB Accession Numbers			
<i>Pseudomonas syringae</i> pv. <i>syringae</i> B728a (Ps)				
OpuC [42]	OpuCD (TMD) Q4ZNI0	OpuCC (SBD) Q4ZNI1	OpuCB (TMD) Q4ZNI2	OpuCA (NBD) Q4ZNI3
<i>Salmonella typhimurium</i> LT2 (St)				
OsmU [43,44]	OsmY (TMD) Q8ZPK1	OsmX (SBD) Q8ZPK2	OsmW (TMD) Q8ZPK3	OsmV (NBD) Q8ZPK4
<i>Staphylococcus aureus</i> Mu50 (Sa)				
OpuC [41]	OpuCA (NBD) A0A0H3JT61	OpuCB (TMD) A0A0H3JT18	OpuCC (SBD) A0A0H3K0Z1	OpuCD (TMD) A0A0H3JU54

¹ Letters in parentheses are the two-letter code used in the main text and in figures; ² Protein subunits are listed in order of their position in the operon; ³ Letters in parentheses indicate domain type (NBD = nucleotide-binding, TMD = transmembrane, SBD = substrate-binding).

Table A2. Top results (Prob ¹ > 50) from searching the PDB using the HHpred server [36] with BileB (residues 1–231) as the query sequence.

PDB ID	Transporter, Substrate, Organism	Prob ¹	E-Value	Cols ²
2ONK_C	ModB ₂ C ₂ A, molybdate, <i>Archaeoglobus fulgidus</i> [69]	99.9	6.60 × 10 ⁻²⁴	209
3D31_C	ModB ₂ C ₂ A, molybdate, <i>Methanosarcina acetivorans</i> [70]	99.9	6.70 × 10 ⁻²⁴	207
3TUI_A	MetNI, methionine, <i>Escherichia coli</i> [71]	99.9	1.90 × 10 ⁻²³	201
4YMU_D	At(QN) ₂ , amino acids, <i>Thermoanaerobacter tengcongensis</i> [72]	99.9	4.10 × 10 ⁻²³	211
4TQU_M	AlgQ2M1M2SS, alginate, <i>Sphingomonas</i> sp. A1 [73]	99.9	6.20 × 10 ⁻²³	209
3RLF_F	MalFGK ₂ , maltose, <i>Escherichia coli</i> [74]	99.9	1.60 × 10 ⁻²⁰	207
3RLF_G	MalFGK ₂ , maltose, <i>Escherichia coli</i> [74]	99.9	1.20 × 10 ⁻²¹	209
4TQU_N	AlgQ2M1M2SS, alginate, <i>Sphingomonas</i> sp. A1 [73]	99.8	2.20 × 10 ⁻²⁰	207

¹ Probability of being a true positive, taking into account a secondary structure score; ² The number of columns in the alignment.

Table A3. Structural homologs of BileB_{SBD} found by searching the PDB using the Dali server [48]. The scores given are from the best match (highest Z-score/lowest RMSD) of individual chain-to-chain comparisons.

PDB ID	Protein ¹	Conformation in Crystal Structure	Z-Score	RMSD (Å) ²
1SW5 [33]	AfProx	open, no ligand	35.4	1.7 (267/270)
3MAM [32]	AfProx	open, ligand-bound (glycine betaine)	34.7	1.6 (267/270)
3O66 ³	SaOpuCC	open, no ligand	34.0	2 (269/272)
4NE4 ³	AtProX	open, no ligand	33.7	1.8 (268/281)
4ND9 ³	AtProX	open, no ligand	33.5	1.7 (267/280)
3PPN [54]	BsOpuCC	open, no ligand	33.4	2.4 (267/270)
4WEP [45]	EcYehZ	open, no ligand	33.0	2 (268/283)
3PPR [54]	BsOpuCC	closed, ligand-bound (ectoine)	30.6	3.9 (269/272)
3PPQ [54]	BsOpuCC	closed, ligand-bound (choline)	30.5	4.2 (269/271)
3PPP [54]	BsOpuCC	closed, ligand-bound (glycine betaine)	30.4	4.2 (269/272)
3PPO [54]	BsOpuCC	closed, ligand-bound (carnitine)	30.0	4.1 (269/272)
1SW2 [33]	AfProX	closed, ligand-bound (glycine betaine)	29.7	4.9 (267/270)
1SW1 [33]	AfProX	closed, ligand-bound (proline betaine)	29.3	4.8 (265/271)
1SW4 [33]	AfProX	closed, ligand-bound (trimethylammonium)	29.2	4.8 (268/270)
3R6U [53]	BsOpuBC	closed, ligand-bound (choline)	27.5	3.8 (247/272)

¹ For full details, including organism names and UniProtKB accession numbers, see Table A1; ² Numbers in parentheses indicate the number of aligned residues/the total number of residues in the matched structure; ³ Deposited as part of the Protein Structure Initiative.

Appendix B.

The amino acid sequence of the recombinant BilEB_{SBD} protein is shown below. The N-terminal tag, containing 10 histidine residues and a TEV protease cleavage site, is underlined. The remaining sequence corresponds to amino acid residues 231–504 of BilEB (UniProt accession Q8Y775).

MHHHHHHHHHHHGENLYFQGSDDKKEITIAGKLGAEPEILINMYKLVIEDETDLKVNVK
 PNMGKTSFVFNALKSGDIDIYPEFTGTVLETFLKENAKTHDPEEVYTQARDGLAKDFDM
 TYLKPMKYNNNTYALAVSPEFAKENNLEKISDLGPVSDQVKAGFTLEFKDRSDGYKGIQDK
 YGLTFSNLKTMPEKLRYNNAIKSGDINLLDAYSTDELAQYKLVLEDDQQLFPPYQGAPL
 MLTKTLDKYPELKKPLNKLKLAGKITDDEM RKMNYEVNVNGKSAYTVAKDYLDQGGIIK

References

- Maertens de Noordhout, C.; Devleeschauwer, B.; Angulo, F.J.; Verbeke, G.; Haagsma, J.; Kirk, M.; Havelaar, A.; Speybroeck, N. The global burden of listeriosis: A systematic review and meta-analysis. *Lancet Infect. Dis.* **2014**, *14*, 1073–1082. [[CrossRef](#)]
- Ferreira, V.; Wiedmann, M.; Teixeira, P.; Stasiewicz, M.J. *Listeria monocytogenes* persistence in food-associated environments: Epidemiology, strain characteristics, and implications for public health. *J. Food Prot.* **2014**, *77*, 150–170. [[CrossRef](#)] [[PubMed](#)]
- Farber, J.M.; Peterkin, P.I. *Listeria monocytogenes*, a food-borne pathogen. *Microbiol. Rev.* **1991**, *55*, 476–511. [[PubMed](#)]
- Walker, S.J.; Archer, P.; Banks, J.G. Growth of *Listeria monocytogenes* at refrigeration temperatures. *J. Appl. Bacteriol.* **1990**, *68*, 157–162. [[CrossRef](#)] [[PubMed](#)]
- McClure, P.J.; Roberts, T.A.; Oguru, P.O. Comparison of the effects of sodium chloride, pH and temperature on the growth of *Listeria monocytogenes* on gradient plates and in liquid medium. *Lett. Appl. Microbiol.* **1989**, *9*, 95–99. [[CrossRef](#)]
- Begley, M.; Gahan, C.G.M.; Hill, C. Bile stress response in *Listeria monocytogenes* LO28: Adaptation, cross-protection, and identification of genetic loci involved in bile resistance. *Appl. Environ. Microbiol.* **2002**, *68*, 6005–6012. [[CrossRef](#)] [[PubMed](#)]
- Gahan, C.G.M.; Hill, C. *Listeria monocytogenes*: Survival and adaptation in the gastrointestinal tract. *Front. Cell. Infect. Microbiol.* **2014**, *4*, 9. [[CrossRef](#)] [[PubMed](#)]
- Sheehan, V.M.; Sleator, R.D.; Hill, C.; Fitzgerald, G.F. Improving gastric transit, gastrointestinal persistence and therapeutic efficacy of the probiotic strain *Bifidobacterium breve* UCC2003. *Microbiology* **2007**, *153*, 3563–3571. [[CrossRef](#)] [[PubMed](#)]
- Watson, D.; Sleator, R.D.; Hill, C.; Gahan, C.G.M. Enhancing bile tolerance improves survival and persistence of *Bifidobacterium* and *Lactococcus* in the murine gastrointestinal tract. *BMC Microbiol.* **2008**, *8*, 176. [[CrossRef](#)] [[PubMed](#)]
- Ruiz, L.; Margolles, A.; Sánchez, B. Bile resistance mechanisms in *Lactobacillus* and *Bifidobacterium*. *Front. Microbiol.* **2013**, *4*, 396. [[CrossRef](#)] [[PubMed](#)]
- Merritt, M.E.; Donaldson, J.R. Effect of bile salts on the DNA and membrane integrity of enteric bacteria. *J. Med. Microbiol.* **2009**, *58*, 1533–1541. [[CrossRef](#)] [[PubMed](#)]
- Begley, M.; Gahan, C.G.M.; Hill, C. The interaction between bacteria and bile. *FEMS Microbiol. Rev.* **2005**, *29*, 625–651. [[CrossRef](#)] [[PubMed](#)]
- Gunn, J.S. Mechanisms of bacterial resistance and response to bile. *Microbes Infect.* **2000**, *2*, 907–913. [[CrossRef](#)]
- Monte, M.J.; Marin, J.J.G.; Antelo, A.; Vazquez-Tato, J. Bile acids: Chemistry, physiology, and pathophysiology. *World J. Gastroenterol.* **2009**, *15*, 804–816. [[CrossRef](#)] [[PubMed](#)]
- Dowd, G.C.; Joyce, S.A.; Hill, C.; Gahan, C.G.M. Investigation of the mechanisms by which *Listeria monocytogenes* grows in porcine gallbladder bile. *Infect. Immun.* **2011**, *79*, 369–379. [[CrossRef](#)] [[PubMed](#)]
- Watson, D.; Sleator, R.D.; Casey, P.G.; Hill, C.; Gahan, C.G.M. Specific osmolyte transporters mediate bile tolerance in *Listeria monocytogenes*. *Infect. Immun.* **2009**, *77*, 4895–4904. [[CrossRef](#)] [[PubMed](#)]

17. Begley, M.; Sleator, R.D.; Gahan, C.G.M.; Hill, C. Contribution of three bile-associated loci, *bsh*, *pva*, and *btlB*, to gastrointestinal persistence and bile tolerance of *Listeria monocytogenes*. *Infect. Immun.* **2005**, *73*, 894–904. [[CrossRef](#)] [[PubMed](#)]
18. Sleator, R.D.; Wemekamp-Kamphuis, H.H.; Gahan, C.G.M.; Abee, T.; Hill, C. A PrfA-regulated bile exclusion system (BilE) is a novel virulence factor in *Listeria monocytogenes*. *Mol. Microbiol.* **2004**, *55*, 1183–1195. [[CrossRef](#)] [[PubMed](#)]
19. Sleator, R.D.; Hill, C. Bacterial osmoadaptation: The role of osmolytes in bacterial stress and virulence. *FEMS Microbiol. Rev.* **2002**, *26*, 49–71. [[CrossRef](#)] [[PubMed](#)]
20. Angelidis, A.S.; Smith, G.M. Role of the glycine betaine and carnitine transporters in adaptation of *Listeria monocytogenes* to chill stress in defined medium. *Appl. Environ. Microbiol.* **2003**, *69*, 7492–7498. [[CrossRef](#)] [[PubMed](#)]
21. Angelidis, A.S.; Smith, G.M. Three transporters mediate uptake of glycine betaine and carnitine by *Listeria monocytogenes* in response to hyperosmotic stress. *Appl. Environ. Microbiol.* **2003**, *69*, 1013–1022. [[CrossRef](#)] [[PubMed](#)]
22. Wemekamp-Kamphuis, H.H.; Sleator, R.D.; Wouters, J.A.; Hill, C.; Abee, T. Molecular and physiological analysis of the role of osmolyte transporters BetL, Gbu, and OpuC in growth of *Listeria monocytogenes* at low temperatures. *Appl. Environ. Microbiol.* **2004**, *70*, 2912–2918. [[CrossRef](#)] [[PubMed](#)]
23. Sleator, R.D.; Hill, C. Compatible solutes: A listerial passe-partout? *Gut Microbes* **2010**, *1*, 77–79. [[CrossRef](#)] [[PubMed](#)]
24. Ter Beek, J.; Guskov, A.; Slotboom, D.J. Structural diversity of ABC transporters. *J. Gen. Physiol.* **2014**, *143*, 419–435. [[CrossRef](#)] [[PubMed](#)]
25. Saurin, W.; Hofnung, M.; Dassa, E. Getting in or out: Early segregation between importers and exporters in the evolution of ATP-binding cassette (ABC) transporters. *J. Mol. Evol.* **1999**, *48*, 22–41. [[CrossRef](#)] [[PubMed](#)]
26. Berntsson, R.P.-A.; Smits, S.H.J.; Schmitt, L.; Slotboom, D.J.; Poolman, B. A structural classification of substrate-binding proteins. *FEBS Lett.* **2010**, *584*, 2606–2617. [[CrossRef](#)] [[PubMed](#)]
27. Scheepers, G.H.; Lycklama A Nijeholt, J.A.; Poolman, B. An updated structural classification of substrate-binding proteins. *FEBS Lett.* **2016**. [[CrossRef](#)] [[PubMed](#)]
28. Obis, D.; Guillot, A.; Gripon, J.C.; Renault, P.; Bolotin, A.; Mistou, M.Y. Genetic and biochemical characterization of a high-affinity betaine uptake system (BusA) in *Lactococcus lactis* reveals a new functional organization within bacterial ABC transporters. *J. Bacteriol.* **1999**, *181*, 6238–6246. [[PubMed](#)]
29. Bouvier, J.; Bordes, P.; Romeo, Y.; Fourçans, A.; Bouvier, I.; Gutierrez, C. Characterization of OpuA, a glycine-betaine uptake system of *Lactococcus lactis*. *J. Mol. Microbiol. Biotechnol.* **2000**, *2*, 199–205. [[PubMed](#)]
30. Fraser, K.R.; Harvie, D.; Coote, P.J.; O’Byrne, C.P. Identification and characterization of an ATP binding cassette L-carnitine transporter in *Listeria monocytogenes*. *Appl. Environ. Microbiol.* **2000**, *66*, 4696–4704. [[CrossRef](#)] [[PubMed](#)]
31. Kappes, R.M.; Kempf, B.; Kneip, S.; Boch, J.; Gade, J.; Meier-Wagner, J.; Bremer, E. Two evolutionarily closely related ABC transporters mediate the uptake of choline for synthesis of the osmoprotectant glycine betaine in *Bacillus subtilis*. *Mol. Microbiol.* **1999**, *32*, 203–216. [[CrossRef](#)] [[PubMed](#)]
32. Tschapek, B.; Pittelkow, M.; Sohn-Bösser, L.; Smits, S.H.J.; Bremer, E.; Schmitt, L. Arg149 is involved in switching the low affinity, open state of the binding protein AfProX into its high affinity, closed state. *J. Mol. Biol.* **2011**, *411*, 36–52. [[CrossRef](#)] [[PubMed](#)]
33. Schiefner, A. Structural basis for the binding of compatible solutes by ProX from the hyperthermophilic archaeon *Archaeoglobus fulgidus*. *J. Biol. Chem.* **2004**, *279*, 48270–48281. [[CrossRef](#)] [[PubMed](#)]
34. Rice, P.; Longden, I.; Bleasby, A. EMBOSS: The European Molecular Biology Open Software Suite. *Trends Genet.* **2000**, *16*, 276–277. [[CrossRef](#)]
35. Tsirigos, K.D.; Peters, C.; Shu, N.; Käll, L.; Elofsson, A. The TOPCONS web server for consensus prediction of membrane protein topology and signal peptides. *Nucleic Acids Res.* **2015**, *43*, W401–W407. [[CrossRef](#)] [[PubMed](#)]
36. Söding, J.; Biegert, A.; Lupas, A.N. The HHpred interactive server for protein homology detection and structure prediction. *Nucleic Acids Res.* **2005**, *33*, W244–W248. [[CrossRef](#)] [[PubMed](#)]
37. Wolters, J.C.; Berntsson, R.P.-A.; Gul, N.; Karasawa, A.; Thunnissen, A.-M.W.H.; Slotboom, D.J.; Poolman, B. Ligand binding and crystal structures of the substrate-binding domain of the ABC transporter OpuA. *PLoS ONE* **2010**, *5*, e10361. [[CrossRef](#)] [[PubMed](#)]

38. Schiefner, A.; Breed, J.; Bösser, L.; Kneip, S.; Gade, J.; Holtmann, G.; Diederichs, K.; Welte, W.; Bremer, E. Cation- π interactions as determinants for binding of the compatible solutes glycine betaine and proline betaine by the periplasmic ligand-binding protein ProX from *Escherichia coli*. *J. Biol. Chem.* **2004**, *279*, 5588–5596. [[CrossRef](#)] [[PubMed](#)]
39. Smits, S.H.J.; Hoing, M.; Lecher, J.; Jebbar, M.; Schmitt, L.; Bremer, E. The compatible-solute-binding protein OpuAC from *Bacillus subtilis*: Ligand binding, site-directed mutagenesis, and crystallographic studies. *J. Bacteriol.* **2008**, *190*, 5663–5671. [[CrossRef](#)] [[PubMed](#)]
40. Horn, C.; Sohn-Bösser, L.; Breed, J.; Welte, W.; Schmitt, L.; Bremer, E. Molecular determinants for substrate specificity of the ligand-binding protein OpuAC from *Bacillus subtilis* for the compatible solutes glycine betaine and proline betaine. *J. Mol. Biol.* **2006**, *357*, 592–606. [[CrossRef](#)] [[PubMed](#)]
41. Kiran, M.D.; Akiyoshi, D.E.; Giacometti, A.; Cirioni, O.; Scalise, G.; Balaban, N. OpuC—An ABC transporter that is associated with *Staphylococcus aureus* pathogenesis. *Int. J. Artif. Organs* **2009**, *32*, 600–610. [[PubMed](#)]
42. Chen, C.; Beattie, G.A. Characterization of the osmoprotectant transporter OpuC from *Pseudomonas syringae* and demonstration that cystathionine-beta-synthase domains are required for its osmoregulatory function. *J. Bacteriol.* **2007**, *189*, 6901–6912. [[CrossRef](#)] [[PubMed](#)]
43. Frossard, S.M.; Khan, A.A.; Warrick, E.C.; Gately, J.M.; Hanson, A.D.; Oldham, M.L.; Sanders, D.A.; Csonka, L.N. Identification of a third osmoprotectant transport system, the OsmU system, in *Salmonella enterica*. *J. Bacteriol.* **2012**, *194*, 3861–3871. [[CrossRef](#)] [[PubMed](#)]
44. Pilonieta, M.C.; Nagy, T.A.; Jorgensen, D.R.; Detweiler, C.S. A glycine betaine importer limits *Salmonella* stress resistance and tissue colonization by reducing trehalose production. *Mol. Microbiol.* **2012**, *84*, 296–309. [[CrossRef](#)] [[PubMed](#)]
45. Lang, S.; Cressatti, M.; Mendoza, K.E.; Coumoundouros, C.N.; Plater, S.M.; Culham, D.E.; Kimber, M.S.; Wood, J.M. YehZYXW of *Escherichia coli* Is a low-affinity, non-osmoregulatory betaine-specific ABC transporter. *Biochemistry* **2015**, *54*, 5735–5747. [[CrossRef](#)] [[PubMed](#)]
46. Kim, S.I.; Ryu, S.; Yoon, H. Roles of YehZ, a putative osmoprotectant transporter, in tempering growth of *Salmonella enterica* serovar Typhimurium. *J. Microbiol. Biotechnol.* **2013**, *23*, 1560–1568. [[CrossRef](#)] [[PubMed](#)]
47. Kabsch, W.; Sander, C. Dictionary of protein secondary structure: Pattern recognition of hydrogen-bonded and geometrical features. *Biopolymers* **1983**, *22*, 2577–2637. [[CrossRef](#)] [[PubMed](#)]
48. Slotboom, D.J.; Duurkens, R.H.; Olieman, K.; Erkens, G.B. Static light scattering to characterize membrane proteins in detergent solution. *Methods* **2008**, *46*, 73–82. [[CrossRef](#)] [[PubMed](#)]
49. ExpASy ProtParam Tool. Available online: <http://web.expasy.org/protparam/> (accessed on 1 November 2016).
50. Holm, L.; Rosenström, P. Dali server: Conservation mapping in 3D. *Nucleic Acids Res.* **2010**, *38*, W545–W549. [[CrossRef](#)] [[PubMed](#)]
51. Mao, B.; Pear, M.R.; McCammon, J.A.; Quijcho, F.A. Hinge-bending in L-arabinose-binding protein. The “Venus’s-flytrap” model. *J. Biol. Chem.* **1982**, *257*, 1131–1133. [[PubMed](#)]
52. PyMOL. Available online: <http://www.pymol.org> (accessed on 1 November 2016).
53. Pittelkow, M.; Tschapek, B.; Smits, S.H.J.; Schmitt, L.; Bremer, E. The crystal structure of the substrate-binding protein OpuBC from *Bacillus subtilis* in complex with choline. *J. Mol. Biol.* **2011**, *411*, 53–67. [[CrossRef](#)] [[PubMed](#)]
54. Du, Y.; Shi, W.W.; He, Y.X.; Yang, Y.H.; Zhou, C.Z.; Chen, Y. Structures of the substrate-binding protein provide insights into the multiple compatible solute binding specificities of the *Bacillus subtilis* ABC transporter OpuC. *Biochem. J.* **2011**, *436*, 283–289. [[CrossRef](#)] [[PubMed](#)]
55. Suzek, B.E.; Huang, H.; McGarvey, P.; Mazumder, R.; Wu, C.H. UniRef: Comprehensive and non-redundant UniProt reference clusters. *Bioinformatics* **2007**, *23*, 1282–1288. [[CrossRef](#)] [[PubMed](#)]
56. Ashkenazy, H.; Abadi, S.; Martz, E.; Chay, O.; Mayrose, I.; Pupko, T.; Ben-Tal, N. ConSurf 2016: An improved methodology to estimate and visualize evolutionary conservation in macromolecules. *Nucleic Acids Res.* **2016**, *44*, W344–W350. [[CrossRef](#)] [[PubMed](#)]
57. Waterhouse, A.M.; Procter, J.B.; Martin, D.M.A.; Clamp, M.; Barton, G.J. Jalview Version 2—A multiple sequence alignment editor and analysis workbench. *Bioinformatics* **2009**, *25*, 1189–1191. [[CrossRef](#)] [[PubMed](#)]
58. Letunic, I.; Bork, P. Interactive tree of life (iTOL) v3: An online tool for the display and annotation of phylogenetic and other trees. *Nucleic Acids Res.* **2016**, *44*, W242–W245. [[CrossRef](#)] [[PubMed](#)]
59. Geertsma, E.R.; Poolman, B. High-throughput cloning and expression in recalcitrant bacteria. *Nat. Methods* **2007**, *4*, 705–707. [[CrossRef](#)] [[PubMed](#)]

60. Kabsch, W. XDS. *Acta Crystallogr. D Biol. Crystallogr.* **2010**, *66*, 125–132. [[CrossRef](#)] [[PubMed](#)]
61. McCoy, A.J.; Grosse-Kunstleve, R.W.; Adams, P.D.; Winn, M.D.; Storoni, L.C.; Read, R.J. Phaser crystallographic software. *J. Appl. Crystallogr.* **2007**, *40*, 658–674. [[CrossRef](#)] [[PubMed](#)]
62. Murshudov, G.N.; Skubák, P.; Lebedev, A.A.; Pannu, N.S.; Steiner, R.A.; Nicholls, R.A.; Winn, M.D.; Long, F.; Vagin, A.A. REFMAC5 for the refinement of macromolecular crystal structures. *Acta Crystallogr. D Biol. Crystallogr.* **2011**, *67*, 355–367. [[CrossRef](#)] [[PubMed](#)]
63. Adams, P.D.; Afonine, P.V.; Bunkóczi, G.; Chen, V.B.; Davis, I.W.; Echols, N.; Headd, J.J.; Hung, L.-W.; Kapral, G.J.; Grosse-Kunstleve, R.W.; et al. PHENIX: A comprehensive Python-based system for macromolecular structure solution. *Acta Crystallogr. D Biol. Crystallogr.* **2010**, *66*, 213–221. [[CrossRef](#)] [[PubMed](#)]
64. Emsley, P.; Lohkamp, B.; Scott, W.G.; Cowtan, K. Features and development of Coot. *Acta Crystallogr. D Biol. Crystallogr.* **2010**, *66*, 486–501. [[CrossRef](#)] [[PubMed](#)]
65. Sievers, F.; Wilm, A.; Dineen, D.; Gibson, T.J.; Karplus, K.; Li, W.; Lopez, R.; McWilliam, H.; Remmert, M.; Söding, J.; et al. Fast, scalable generation of high-quality protein multiple sequence alignments using Clustal Omega. *Mol. Syst. Biol.* **2011**, *7*, 539. [[CrossRef](#)] [[PubMed](#)]
66. EMBL-EBI Clustal Omega Server. Available online: <http://www.ebi.ac.uk/Tools/msa/clustalo/> (accessed on 1 November 2016).
67. Gouveia-Oliveira, R.; Sackett, P.W.; Pedersen, A.G. MaxAlign: Maximizing usable data in an alignment. *BMC Bioinform.* **2007**, *8*, 312. [[CrossRef](#)] [[PubMed](#)]
68. Ko, R.; Smith, L.T. Identification of an ATP-driven, osmoregulated glycine betaine transport system in *Listeria monocytogenes*. *Appl. Environ. Microbiol.* **1999**, *65*, 4040–4048. [[PubMed](#)]
69. Hollenstein, K.; Frei, D.C.; Locher, K.P. Structure of an ABC transporter in complex with its binding protein. *Nature* **2007**, *446*, 213–216. [[CrossRef](#)] [[PubMed](#)]
70. Gerber, S.; Comellas-Bigler, M.; Goetz, B.A.; Locher, K.P. Structural basis of trans-inhibition in a molybdate/tungstate ABC transporter. *Science* **2008**, *321*, 246–250. [[CrossRef](#)] [[PubMed](#)]
71. Johnson, E.; Nguyen, P.T.; Yeates, T.O.; Rees, D.C. Inward facing conformations of the MetNI methionine ABC transporter: Implications for the mechanism of transinhibition. *Protein Sci.* **2012**, *21*, 84–96. [[CrossRef](#)] [[PubMed](#)]
72. Yu, J.; Ge, J.; Heuveling, J.; Schneider, E.; Yang, M. Structural basis for substrate specificity of an amino acid ABC transporter. *Proc. Natl. Acad. Sci. USA* **2015**, *112*, 5243–5248. [[CrossRef](#)] [[PubMed](#)]
73. Maruyama, Y.; Itoh, T.; Kaneko, A.; Nishitani, Y.; Mikami, B.; Hashimoto, W.; Murata, K. Structure of a bacterial ABC transporter involved in the import of an acidic polysaccharide alginate. *Structure* **2015**, *23*, 1643–1654. [[CrossRef](#)] [[PubMed](#)]
74. Oldham, M.L.; Chen, J. Snapshots of the maltose transporter during ATP hydrolysis. *Proc. Natl. Acad. Sci. USA* **2011**, *108*, 15152–15156. [[CrossRef](#)] [[PubMed](#)]



© 2016 by the authors; licensee MDPI, Basel, Switzerland. This article is an open access article distributed under the terms and conditions of the Creative Commons Attribution (CC-BY) license (<http://creativecommons.org/licenses/by/4.0/>).